

Scoring Multipole Electrostatics in Condensed-Phase Atomistic Simulations

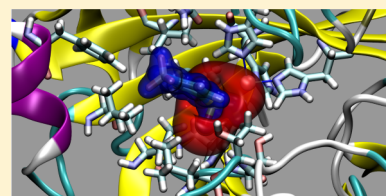
Tristan Bereau,^{*,†} Christian Kramer,^{†,‡,§} Fabien W. Monnard,[†] Elisa S. Nogueira,[†] Thomas R. Ward,[†] and Markus Meuwly^{*,†}

[†]Department of Chemistry, University of Basel, 4056 Basel, Switzerland

[‡]Novartis Institutes for BioMedical Research, Basel, Switzerland

S Supporting Information

ABSTRACT: Permanent multipoles (MTPs) embody a natural extension to common point-charge (PC) representations in atomistic simulations. In this work, we propose an alternative to the computationally expensive MTP molecular dynamics simulations by running a simple PC simulation and later reevaluate—“score”—all energies using the more detailed MTP force field. The method, which relies on the assumption that the PC and MTP force fields generate closely related phase spaces, is accomplished by enforcing identical sets of monopoles between the two force fields—effectively highlighting the higher MTP terms as a correction to the PC approximation. We first detail our consistent parametrization of the electrostatics and van der Waals interactions for the two force fields. We then validate the method by comparing the accuracy of protein–ligand binding free energies from both PC and MTP-scored representations with experimentally determined binding constants obtained by us. Specifically, we study the binding of several arylsulfonamide ligands to human carbonic anhydrase II. We find that both representations yield an accuracy of 1 kcal/mol with respect to experiment. Finally, we apply the method to rank the energetic contributions of individual atomic MTP coefficients for molecules solvated in water. All in all, MTP scoring is a computationally appealing method that can provide insight into the multipolar electrostatic interactions of condensed-phase systems.



INTRODUCTION

The realm of point-charge (PC) electrostatics in atomistic simulations has provided a phenomenal amount of insight for various biochemical systems—proteins,^{1–6} membranes,⁷ and viruses,^{8,9} to name but a few. Originating from a first-order expansion of the electrostatic potential (ESP; see below for details), it assigns a partial charge to each atomic site—effectively summing over nuclear charge and electron cloud. While such an endeavor is straightforward for monatomic ions, complications arise for polyatomic ions and molecules. The PC approximation has shown its limitations¹⁰ for the description of specific chemical systems, e.g., cation– π interactions¹¹ or halogen bonds.¹² As a result, a number of methods have been proposed to go beyond the simple PC approximation, including: (i) off-center charges placed along bonds or lone pairs;^{13,14} (ii) atomic polarizabilities;^{15–17} and (iii) atomic multipoles (MTPs).^{17–19} Focusing on the description of permanent MTPs, methods (i) and (iii) vary greatly: While off-center charges only require a limited number of additional particles—making the method computationally appealing—recreating MTPs by setting an adequate set of off-site, charged particles (e.g., two nearby charges of equal strength and opposite sign to emulate a dipole moment) requires a great deal of care in the parametrization. On the other hand, the explicit inclusion of permanent MTPs in a molecular dynamics (MD) simulation is considerably more computationally expensive and has thus been, so far, limited to either gas-phase or small condensed-phase systems.^{20,21} Indeed, considering that an

atomic MTP description up to quadrupoles requires 9 coefficients (i.e., 1 for the monopole, 3 for the dipole, 5 for the quadrupole; see below and ref 19), this enforces 9×9 interactions per atom pair—compared to 1×1 in the simple PC approximation. Adding up the extra computational overhead associated with local axis-system calculations^{17,19,22} and various geometrical factors, one easily reaches a computational slowdown on the order of 10^3 —a steep price considering that statistical sampling of modest-size systems with PC is still very much a critical issue.²³

In the present work, we propose, test, and validate an alternative approach to incorporate atomic MTPs offering both a systematic parametrization scheme and moderate extra computational cost. Building on the idea that a MTP expansion is a higher-order correction of the ESP compared to a PC approximation (see eq 8), these two expansions should converge in the limit where the magnitude of the nonmonopole coefficients approaches zero. As a result, the Hamiltonians generated by the two electrostatic representations would sample similar phase spaces and thus the same distribution of conformations. We point out the analogy with the MM-GBSA calculation technique (see, e.g., ref 24 and references therein), in which one typically estimates a protein–ligand binding free energy from a single simulation of the complex and assumes

Received: January 18, 2013

Revised: April 4, 2013

Published: April 5, 2013

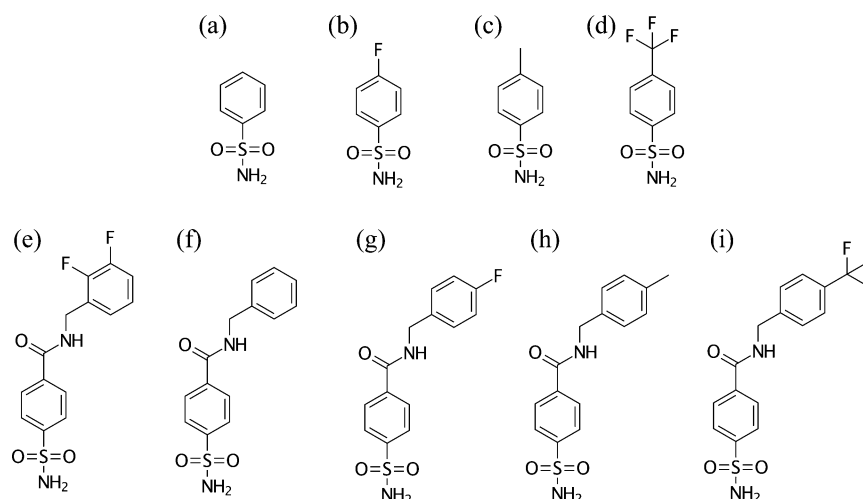


Figure 1. Structures of the (fluoro-)arylsulfonamide inhibitors studied in the present work. The first four ligands (top) correspond to benzene sulfonamide (BZS) derivatives: (a) BZS, (b) 4-fluoro-BZS (F-BZS), (c) 4-methyl-BZS (CH₃-BZS), and (d) 4-fluoro-methyl-BZS (CF₃-BZS). The last five ligands (bottom) correspond to 4-(aminosulfonyl)-*N*-phenylmethybenzamide derivatives (SBB): (e) 2,3-difluoro-SBB (F₂-SBB), (f) SBB, (g) 4-fluoro-SBB (F-SBB), (h) 4-methyl-SBB (CH₃-SBB), and (i) 4-fluoro-methyl-SBB (CF₃-SBB). Note that, upon binding, all sulfonamide groups deprotonate, resulting in a net charge.

that it reproduces the distribution of conformations of the individual monomers. This equivalence between Hamiltonians would ensure the ability to run a MD simulation with one force field and later reevaluate the energies using the second—a method we refer to as “scoring”. We hereby employ to score PC-generated trajectories using a MTP force field. By parametrizing both PC and MTP force fields, we can ensure that monopole coefficients are assigned virtually identical values—this naturally scales down the strength of the nonmonopole coefficients during optimization—which in turn provides the necessary ingredients for the scoring method.

In this work, we study the scope in which MTP scoring yields reliable results. The calculation of protein–ligand binding free energies is an excellent means to evaluate the accuracy of electrostatic representations, mainly due to the delicate interactions between ligand, protein, and the surrounding water. We set out to calculate the binding of a series of arylsulfonamide ligands (see Figure 1)^{25–27} to human carbonic anhydrase II (hCA II), a widely studied metalloenzyme that catalyzes the reversible hydration of carbon dioxide.²⁵ To evaluate the accuracy of our methodology, we have experimentally measured the same set of binding affinities using enzyme-assay techniques. Relying on a series of measurements performed in the *same* laboratory provides consistency in the results—a critical consideration as significant discrepancies commonly arise from one protocol to the next.²⁸ To cancel some of these systematic errors, as well as help converge the free-energy calculations, we focus on *relative* free energies of binding between two ligands. Free-energy calculations were based on the thermodynamically correct free-energy perturbation (FEP) approach²⁹—a gold standard for accurate predictions of binding free energies.³⁰

Andrienko and co-workers have relied on such a scoring technique to calculate the electrostatic energy of charged molecules in the context of organic semiconductors, using both Thole’s interacting polarizability model and permanent MTP coefficients.^{31,32} We note that their typical energy shifts lie in the electronvolt regime, whereas the present calculations of protein–ligand binding free energies operate at the kilo-

calories/mole level (1 eV \approx 23 kcal/mol), which allows us to probe subtle energy variations.

In the current study, we will parametrize and validate both PC and MTP force fields, run FEP calculations with PCs, score the trajectories with the MTP force field, and compare both PC and MTP free energies to the experimentally determined binding constants. Finally, the MTP scoring method will be applied to gain insight into the multipolar electrostatics of C–H and C–F groups solvated in water.

METHODS

Simulation Protocol. To compare PC and MTP force fields, we seek to parametrize both in a consistent way. Because reparametrizing the entire water–ligand–protein system struck us as daunting, we instead fixed the water and protein force fields using CHARMM22 with CMAP corrections³³ and focused exclusively on the ligands. Our work illustrates that a careful reparametrization of the ligand alone, combined with standard mixing rules, goes a long way in properly describing protein–ligand binding.

All simulations were run in NAMD 2.8³⁴ using a $\Delta t = 1$ fs time step; the SHAKE algorithm³⁵ on water molecules; Particle-Mesh Ewald (PME) with grid-size spacing of 1 Å, relative tolerance of 10^{-6} , and interpolation order 4 for long-range electrostatics; and a 12 Å cutoff and 11 Å switching for the Lennard-Jones interactions. Temperature control was applied using a Langevin thermostat at 300 K (unless stated otherwise) and friction coefficient $\gamma = 1$ ps^{−1}. Simulations in water were additionally coupled to a modified Nosé–Hoover method with Langevin-type barostat fluctuations, targeting atmospheric pressure (i.e., 1.01325 bar), and set to an oscillation period of 100 fs and a damping time scale of 50 fs.

Water simulations were set by solvating a compound in a box of size $L \approx 25$ Å. The simulation box was (i) energy minimized for 5000 steps of conjugate gradient, (ii) heated incrementally to 300 K over 4 ps, and (iii) equilibrated for 50 ps. Charged compounds were neutralized using a sodium counterion; we avoided strong electrostatic artifacts by applying a “half-harmonic”-like lower bound restraint between the counterion

and the compound of interest, using a minimum length of 12.5 Å and force constant of 5 kcal/mol·Å².

The starting structure is hCA II with a fluorinated, aryl-sulfonamide ligand (PDB code 1G54²⁷). Minimal energy structures of our ligands (Figure 1) were docked into the protein by best aligning the aryl-sulfonamide groups. The protein–ligand complex was solvated in a box of size $L \approx 80$ Å and neutralized with sodium counterions. A similar minimization/heating/equilibrium process was applied using 8 ps of heating time and 1 ns of equilibration for each ligand. A series of angle and dihedral restraints were applied between the sulfonamide group of the ligand and the Zn(His)₃ moiety of hCA II, following the protocol applied in a previous study.²⁶

Free-Energy Calculations. Hydration and protein–ligand binding free energies were calculated using free energy perturbation (FEP) techniques,²⁹ where one gradually couples/decouples chemical groups from the rest of the system using a parameter λ_i that scales the relevant nonbonded interactions. The Bennett Acceptance Ratio (BAR)³⁶ allows us to calculate the free energy difference associated with the alchemical transformation from Boltzmann-weighted energy differences between N consecutive Hamiltonians $\mathcal{H}(\lambda_i)$

$$\Delta G_{A \rightarrow B} = -\beta^{-1} \sum_{i=1}^{N-1} \ln \langle \exp \{ -\beta [\mathcal{H}(\lambda_{i+1}) - \mathcal{H}(\lambda_i)] \} \rangle_i \quad (1)$$

where $A \rightarrow B$ refers to the alchemical transformation between compounds A and B (e.g., BZS \rightarrow CF₃-BZS); $\beta^{-1} = k_B T$; and the canonical average $\langle \cdot \rangle_i$ is performed over the phase space generated by $\mathcal{H}(\lambda_i)$.

Following previously published protocols,^{37–39} we couple/decouple electrostatics and Lennard-Jones interactions in a sequential manner: they are turned on/off in the intervals $0 < \lambda < 0.5$ and $0.5 < \lambda < 1$, respectively. We have obtained good convergence using this scheme: no simulation required the annihilation or exnihilation of net charges, which typically involve simulation-protocol caveats and large free-energy differences. The use of soft-core potentials prevented steric clashes when tuning λ close to 0 or 1 as they allow a gradual scaling of the nonbonded interactions. We used a van der Waals (VDW) radius-shifting coefficient $\delta = 5.0$ Å². Shirts et al. have demonstrated the importance of applying long-range VDW corrections in FEP calculations.³⁷ Considering that (i) this work focuses on a comparison between electrostatic representations and (ii) these long-range corrections are of the same magnitude as the error associated with analyzing a NAMD simulation in CHARMM (see below), we neglected this contribution.

Hydration and protein–ligand-binding free energies were calculated using standard thermodynamic cycles.^{40,41} We calculated absolute hydration free energies of a compound by performing a single simulation in water while decoupling the intramolecular energies. Relative protein–ligand-binding free energies were calculated by performing alchemical transformations between two ligands in both water and the solvated protein environment: $\Delta \Delta G_{\text{bind}} = \Delta \Delta G_{\text{port}} - \Delta \Delta G_{\text{wat}} = -k_B T_{\text{room}} \ln(K_j/K_i)$, where the last expression relates to experimentally determined dissociation constants of ligands i and j .

Simulation windows were set every $\lambda = 0.02$, except close to 0 and 1 where we used logarithmically distributed λ values (i.e., $\lambda \in \{0, 0.00001, 0.0001, 0.001, 0.01, 0.02, 0.04, \dots, 0.96, 0.98,$

$0.99, 0.999, 0.9999, 0.99999, 1\}$) to account for possibly large changes in these regions. We ran 100 ps of simulation for each window, including 50 ps of equilibration time. Each FEP calculation was run in both directions (i.e., forward and backward). Not only did this allow us to check their convergence, we also used them to crudely estimate the statistical error associated with our calculations, rather than relying on more elaborate techniques (e.g., bootstrap resampling⁴²)

MTP Scoring. MTP scoring was performed by reading NAMD trajectories and reevaluating energies at each time step using the MTP force field on the ligand while keeping PC electrostatics for the rest of the system (i.e., counterions, water, protein). This scoring was performed within CHARMM⁴³ using an in-house MTP energy calculation module. While the NAMD simulations were performed with PME, our current MTP-electrostatics implementation does not include any corresponding method (this has been described elsewhere⁴⁴). Instead of evaluating the electrostatic energies with periodic boundary conditions and spherical cutoffs, we have obtained better stability using a nearest-image convention—Rühle et al. also observed good convergence properties using this protocol.³¹ VDW energies, unlike the MTP electrostatics, relied on soft-core potentials—as in the NAMD simulations. For consistency, all free-energy calculations presented in this work were calculated exclusively from CHARMM, whether using the PC or MTP force fields. We found that corresponding free-energy calculations (i.e., only for PC) evaluated from NAMD and CHARMM deviated from one another by no more than 0.3 kcal/mol (data not shown)—an acceptable discrepancy considering the differences in their treatment of electrostatics.

The FEP scoring protocol of a trajectory consisted of four independent contributions: (i) E_{vdW} , the total VDW energy with all electrostatics turned off; (ii) $E_{\text{elec}}^{\text{env}}$, the PC electrostatic energy of everything but the alchemically transformed groups; (iii) $E_{\text{elec}}^{\text{exn}}$, the MTP electrostatic energy of the exnihilated group; and (iv) $E_{\text{elec}}^{\text{ann}}$, the MTP electrostatic energy of the annihilated group. These terms are combined according to the snapshot's λ_i and λ_{i+1}

$$\mathcal{H}(\lambda_{i+1}) - \mathcal{H}(\lambda_i) = E_{\text{vdW}}(\lambda_{i+1}) - E_{\text{vdW}}(\lambda_i) + E_{\text{elec}}(\lambda_{i+1}) - E_{\text{elec}}(\lambda_i) \quad (2)$$

where

$$E_{\text{elec}}(\lambda) = \begin{cases} 2\left(\frac{1}{2} - \lambda\right)(E_{\text{elec}}^{\text{ann}} - E_{\text{elec}}^{\text{env}}), & \text{if } \lambda < 1/2 \\ 2\left(\lambda - \frac{1}{2}\right)(E_{\text{elec}}^{\text{exn}} - E_{\text{elec}}^{\text{env}}), & \text{otherwise} \end{cases} \quad (3)$$

Note that $E_{\text{vdW}}(\lambda)$ is the soft-core VDW potential

$$E_{\text{vdW}}(\lambda) = \lambda \epsilon_{ij} \left[\left(\frac{R_{ij}^{\min 2}}{r_{ij}^2 + \delta(1 - \lambda)} \right)^6 - 2 \left(\frac{R_{ij}^{\min 2}}{r_{ij}^2 + \delta(1 - \lambda)} \right)^3 \right] \quad (4)$$

and the dependence of $E_{\text{elec}}(\lambda)$ on λ explicitly refers to the way annihilated and exnihilated atoms are decoupled/coupled to the simulation cell in this work. Note that $E_{\text{elec}}^{\text{ann,env,exn}}$ corresponds to the original PC/MTP energy.¹⁹ These contributions are

combined according to the BAR equation (eq 1) to yield the scored free energy.

Experimental Binding Affinity Determination. The wild-type hCA II was produced and purified according to ref 45. All BZS ligands were purchased while the SBB ligands were synthesized (the NMR spectral assignment is provided in the Supporting Information). Because of the various strengths in binding affinity of the ligands studied in this work (Figure 1), two experimental assays were used: (i) esterase activity for the BZS ligands (described in ref 26 and the Supporting Information) and (ii) competitive displacement for the SBB ligands (below). The resulting binding constants for all ligands are presented in Table 1.

Table 1. Inhibition/Dissociation Constants, $K_{i/d}$, Determined for the BZS and SBB Ligands and DNSA, As Well As the Corresponding Free Energy, $\Delta G = +k_B T_{\text{room}} \ln K_{i/d}$, Expressed in kcal/mol^a

inhibitor	this work		previous work	
	$K_{i/d}$ [nM]	ΔG [kcal/mol]	$K_{i/d}$ [nM]	PDB
BZS	779 \pm 45 ^a	−8.38 \pm 0.03	200–1500 ^{46,47}	—
F-BZS	326 \pm 30 ^a	−8.90 \pm 0.05	82 ⁴⁷	—
CH ₃ -BZS	491 \pm 13 ^a	−8.66 \pm 0.02	590 ⁴⁸	1IF4
CF ₃ -BZS	28.5 \pm 3.2 ^b	−10.35 \pm 0.06	—	—
SBB	1.7 \pm 0.2 ^b	−12.03 \pm 0.07	—	—
F-SBB	2.2 \pm 0.2 ^b	−11.88 \pm 0.05	3.3 ⁴⁹	—
CH ₃ -SBB	2.3 \pm 0.2 ^b	−11.85 \pm 0.05	—	—
F ₂ -SBB	1.9 \pm 0.2 ^b	−11.97 \pm 0.06	1.1 ⁵⁰	1G4O
CF ₃ -SBB	2.5 \pm 0.2 ^b	−11.81 \pm 0.05	0.3 ⁵¹	1G52
DNSA	1630 \pm 60 ^b	−7.94 \pm 0.02	826 ⁵²	1OKL

^aWhen available, values from published work are shown for comparison, as well as PDB structures of the corresponding hCA II–ligand complex. Superscripts *a* and *b* refer to the esterase activity and competitive displacement assays, respectively. Experimental methods *a* and *b* extracted K_i and K_d values, respectively.

The competitive displacement of the fluorescent hCA II inhibitor dansylamide (DNSA) was used to determine dissociation constants, K_d , of the strongly binding ligands. DNSA is nonfluorescent in aqueous solution but emits a signal at 470 nm in the presence of the protein (excitation at 280 nm). We determined K_d values from a modified method proposed by Tripp and co-workers,^{53–55} where a Nunc 96-well, black polystyrene plate was used with excitation at 280 nm and detection at 490 nm. The K_d for DNSA was determined by titrating 100 nM of hCA II by varying its concentration $[D]$ from 0.05 to 100 μ M of DNSA in a total volume of 208 μ L (Figure S2, Supporting Information). The equilibrium dissociation constant for DNSA, $K_d^{(\text{DNSA})}$, was determined by fitting the fluorescence data using

$$F_{\text{tot}} = \frac{F_{\text{obs}} - F_{\text{ini}}}{F_{\text{end}} - F_{\text{ini}}} = \frac{1}{1 + K_d^{(\text{DNSA})}/[D]} \quad (5)$$

where F_{tot} is the total fluorescence; F_{obs} is the inhibitor-concentration-dependent fluorescence signal; F_{ini} is the initial fluorescence of hCA II in the absence of DNSA; and F_{end} is the end-point fluorescence. We then titrated a fixed concentration of DNSA ($[D] = 2.25 \mu\text{M}$) against each inhibitor from 100 μM to 25 nM and subsequently extracted K_d from

$$F_{\text{tot}} = \frac{F_{\text{obs}} - F_{\text{ini}}}{F_{\text{end}} - F_{\text{ini}}} = \frac{1}{1 + (K_d^{(\text{DNSA})}/[D])(1 + [I]/K_d)} \quad (6)$$

where $[I]$ is the inhibitor's concentration. Normalized fluorescence activity curves for the SBB and the CF₃-BZS ligands are shown in Figure S3 (Supporting Information).

■ FORCE-FIELD PARAMETRIZATION

In the following, we describe our protocol to parametrize the present set of sulfonamide ligands. These include bonded, electrostatic, and VDW interactions. Most bonded parameters were taken from the CHARMM22 force field with CMAP corrections.³³ Parameters for fluorinated groups were taken from a separate optimization study.⁵⁶ For simplicity, all bonded parameters were subsequently kept fixed when reparametrizing nonbonded interactions.

Electrostatic Interactions. The present work follows the notation of Stone.¹⁹ We consider a localized charge density $\rho(\mathbf{x}')$ generating an electrostatic potential (ESP) $\Phi(\mathbf{x})$ at position \mathbf{x}

$$4\pi\epsilon_0\Phi(\mathbf{x}) = \int d\mathbf{x}' \frac{\rho(\mathbf{x}')}{|\mathbf{x} - \mathbf{x}'|} \quad (7)$$

A Taylor series expansion of $1/R \equiv 1/|\mathbf{x} - \mathbf{x}'|$ provides the following multipole expansion for Φ in Cartesian coordinates

$$4\pi\epsilon_0\Phi(\mathbf{x}) = q\left(\frac{1}{R}\right) + \frac{\mu_\alpha R_\alpha}{R^3} + \frac{1}{3}\Theta_{\alpha\beta} \frac{3R_\alpha R_\beta - R^2\delta_{\alpha\beta}}{R^5} + \dots \quad (8)$$

where μ_α is the component α of the dipole moment μ , $\Theta_{\alpha\beta}$ is the component $\alpha\beta$ of the second-rank quadrupole moment tensor Θ , and the Einstein summation convention is applied.

Extending the work of Kramer et al.,²² we parametrize multipole moments on each atomic site of a given molecule to best reproduce its ESP between the Lee-Richards molecular surfaces⁵⁷ of 1.66 σ and 2.2 σ , where σ is an atomic site's VDW radius. The ESP is then approximated by a sum over all multipole moments—up to the quadrupole terms in this work—assigned to each atomic site *a* of a molecule where superscript (*a*) denotes a dependence to the *a*th atomic site. We express the ESP by grouping atoms of identical type *t*

$$4\pi\epsilon_0\Phi(\mathbf{x}) \simeq \sum_{t=1}^{N_t} \left[q^{(t)} \left(\sum_{a_i \in t} \frac{1}{R^{(a_i)}} \right) + \mu_\alpha^{(t)} \left(\sum_{a_i \in t} \frac{R_\alpha^{(a_i)}}{R^{(a_i)3}} \right) + \frac{1}{3} \Theta_{\alpha\beta}^{(t)} \left(\sum_{a_i \in t} \frac{3R_\alpha^{(a_i)} R_\beta^{(a_i)} - R^2 \delta_{\alpha\beta}}{R^{(a_i)5}} \right) \right] \quad (9)$$

As described below, our atom-typing scheme takes into account not only the chemical element of the atom but also its local environment. Grouping atoms in types allows us to circumvent fitting problems associated with buried atoms (i.e., for which the solvent is not accessible), which lack nearby ESP grid points for a proper convergence of their PC/MTP coefficients. This was previously addressed in the RESP algorithm by assigning harmonic restraints to non-hydrogen atoms.⁵⁸ Here, we instead rely on the redundancy of atom types over different molecules/conformations, which helps sample a sufficient number of ESP grid points from a variety of geometries. The downside of fitting several molecules/conformations at once is that it

amplifies the weight difference between exposed and buried atom types during the fit (described below). A strong imbalance between atom-type weights means that a few over-represented parameters will drive the fit, while varying the parameters of others will only marginally affect the target function. To alleviate this overamplification, we restrained the PC parameters to the average value of fits to the individual molecules/conformations (details below). Moreover, a simultaneous fit of multiple molecules using this atom-typing scheme allows us to derive consistent electrostatic parameters between alchemically transformed molecules. Effectively, this keeps the PC/MTP parameters of all persistent (i.e., nonsubstituted) atoms fixed, except for one atom that connects the persistent to the alchemically transformed groups; e.g., a H \rightarrow F alchemical transformation on a benzene ring would affect not only the PC/MTP coefficients of the two atoms but also the carbon that is connected to both, thereby ensuring a correct net charge in each case.

In the following, all multipole moments will be expressed in spherical coordinates Q_{lk} , where l denotes the order of the expansion and k is used to iterate over the $2l + 1$ coefficients:¹⁹

$l = 0$: The charge q is invariant under coordinate transformation: $Q_{00} = q$.

$l = 1$: The dipole moment μ becomes $Q_{10} = \mu_z$; $Q_{11c} = \mu_x$; and $Q_{11s} = \mu_y$.

$l = 2$: The symmetry and traceless property of Θ imply that only five coefficients characterize the quadrupole moment: $Q_{20} = \Theta_{zz}$; $Q_{21c} = 2\Theta_{xz}/\sqrt{3}$; $Q_{21s} = 2\Theta_{yz}/\sqrt{3}$; $Q_{22c} = (\Theta_{xx} - \Theta_{yy})/\sqrt{3}$; and $Q_{22s} = 2\Theta_{xy}/\sqrt{3}$.

Fitting Protocol. Equation 9 shows that the ESP is expressed as a linear combination of the multipoles Q_{lk} . From a collection of points \mathbf{x}_i at which the ESP is evaluated, one can linearly optimize the set of coefficients Q_{lk}

$$\sum_{i=1}^{N_i} \sum_{l=0}^2 \sum_{k=0}^{2l+1} A_{lk,i}^{(t)} Q_{lk}^{(t)} = 4\pi\epsilon_0 \Phi(\mathbf{x}_i) \quad (10)$$

which can simply be expressed in matrix notation as $\mathbf{A}\mathbf{y} = \mathbf{b}$, where \mathbf{A} is an $m \times n$ matrix—with $n \ll m$ —containing m ESP grid points and n geometrical factors $A_{lk,i}^{(t)}$ that multiply with their corresponding coefficient $Q_{lk}^{(t)}$ —denoted as \mathbf{y} —(e.g., point charge, dipole moments) of atom type t . \mathbf{b} is a vector of length m that contains the values of the ESP at each grid point. As we fit the electrostatic interaction parameters of multiple molecules at once, a given atom type is usually only present in a few molecules, thus only sampled from a subset of ESP grid points. In general, \mathbf{A} will thus tend to a sparse matrix as additional molecules are incorporated. We reduce the dimensionality of the problem by solving the equivalent problem $\mathbf{A}^T \mathbf{A} \mathbf{y} = \mathbf{A}^T \mathbf{b}$, where \mathbf{A}^T is \mathbf{A} 's transpose. The matrix product $\mathbf{A}^T \mathbf{A}$ is of size $n \times n$ —a significant computational improvement over \mathbf{A} . We performed the linear optimization using a conjugate gradient algorithm. ESP grid points were calculated from ab initio single-point calculations at the MP2/6-311G(d,p) level using Gaussian 09.⁵⁹

Three types of penalties were applied to the fit:

1. A charge control—applied to the $Q_{00}^{(t)}$ parameters—enforced the correct net charge for each molecule: $\sum_t \lambda_{cc} N_j^{(t)} = \lambda_{cc} q_j^{\text{tot}}$, where $N_j^{(t)}$ is the number of atoms of atom type t contained in molecule j ; λ_{cc} is the charge-control penalty prefactor; and q_j^{tot} is molecule j 's net charge. λ_{cc} was iteratively increased until the maximum charge deviation (i.e., between the

net and the calculated charges) converged—typically reaching values in the range 10^{-13} – 10^{-15} .

2. The above-mentioned predominant weight of certain atom types in the combined fit was addressed by first deriving PC parameters for all molecules independently. We then fitted simultaneously all molecules and applied a penalty to restrain the PCs within the average values of the individual fits across all molecules. The penalty was iteratively increased until all monopoles fell within 0.1 e of their target value.

3. In light of our motivation to derive MTP electrostatics that represent a *refinement* of a PC approximation, we also restrained the monopole coefficients (i.e., $l = 0$) of MTP fits to a maximum of 0.005 e deviation from the PC-optimized coefficients. While this restraint will limit the improved accuracy one can gain from a MTP representation—a comparison is provided below—the resulting parametrization better interfaces with the PC-only force field for the protein and the water. This subsequently allows for energy calculations where the MTP force field for the ligand is used in combination with the PC force field for the rest of the system. Evidently, restraining the monopole coefficients will tend to scale down the strength of the nonmonopole coefficients compared to an unrestricted fit.

Additionally, we limit the MTP expansion of hydrogen atoms to monopoles only throughout this work.

Atom Types and Reference Axis System. Atom typing involved: (i) the chemical element of a given atom; (ii) its connectivity to neighboring atoms (up to 4); and (iii) the chemical elements of these neighboring atoms. These conditions not only define specific atom types that vary according to the atoms' chemical environment but also provide a reference axis system. This axis system is used below to express the dipole and quadrupole moments of each atom. More details on atom typing and reference axis systems can be found in Kramer et al.²²

We express an atom type followed by up to four neighbors using the following notation: (i) the chemical element (e.g., “H” for hydrogen, “Car” for aromatic carbon), (ii) the number of bonded neighbors, and (iii) a + or – sign if a neighboring charge is present. Optimized PC and MTP coefficients are listed in the Supporting Information (Table S1). Overall, the root-mean-squared errors (RMSEs) between the ab initio and fitted ESPs were 1.95, 1.31, and 0.85 kcal/mol for the following parametrizations: PC, MTP with all penalties, and MTP with all penalties but #3, respectively. The last parametrization scheme was not used in the remainder of this paper because it fails to enforce similar phase spaces between PC and MTP, thus thwarting the applicability of the MTP scoring method.

van der Waals Interactions. Since force fields must ultimately strike an exquisite balance between electrostatics and VDW interactions, we have found it necessary to systematically reoptimize *both* terms.

VDW interactions are described by Lennard-Jones (LJ) potentials

$$U_{LJ} = \sum_{ij} \epsilon_{ij} \left[\left(\frac{R_{ij}^{\min}}{r_{ij}} \right)^{12} - 2 \left(\frac{R_{ij}^{\min}}{r_{ij}} \right)^6 \right] \quad (11)$$

where ϵ_{ij} and R_{ij}^{\min} scale the interaction strength and range, respectively, between atoms i and j . We parametrized the coefficients pertaining to individual atoms (i.e., ϵ_i , R_i^{\min}) and applied the Lorentz–Berthelot mixing rule, which assigns atom-

pair interaction range and strength coefficients using the arithmetic and geometric mean of the individual coefficients, respectively.

In addition to ab initio calculations, VDW parametrization schemes typically rely on empirically determined thermodynamic data (e.g., heat of vaporization)^{58,60,61}—a common approach to alleviate problems associated with limitations in the accurate calculation of dispersion interactions from ab initio calculations.⁶² Here, we follow the same route by optimizing both (i) intermolecular energies of a model compound with one water molecule and (ii) experimentally determined pure-liquid densities.

Ab Initio Calculations. Dimer conformations of compound–water complexes were first generated from a 1 ns long NPT simulation using the standard CHARMM22 force field. The compound was solvated in a box of TIP3P water molecules, and 1000 dimer complexes were extracted at regular time intervals. We only retained water molecules within the first solvation shell of the compound for parametrization reasons: (i) reproducing dimer energies at large distances (i.e., $r_{ij} \gg R_{ij}^{\text{min}}$) provides little information on the LJ coefficients because all LJ interactions are close to zero and (ii) short dimer distances (i.e., $r_{ij} \gg R_{ij}^{\text{min}}$) are only sensitive to the rapidly varying, repulsive part of the potential, which are both hardly ever sampled (i.e., $U \gg k_B T_{\text{room}}$) and difficult to fit. The extracted dimer conformations were then calculated from Gaussian 09⁵⁹ at the MP2 level of theory using a 6-311G(d,p) basis set and basis-set superposition error (BSSE) correction.

The LJ parameters were optimized by subsequently minimizing the following two target functions

$$\chi_1^2 = \sum_i w_1^i (\Delta E_{\text{QM}}^i - \Delta E_{\text{elec}}^i - \Delta E_{\text{LJ}}^i)^2 \quad (12)$$

$$\chi_2^2 = \sum_i w_2^i (\Delta E_{\text{QM}}^i - \Delta E_{\text{elec}}^i - \Delta E_{\text{LJ}}^i)^2 \quad (13)$$

where ΔE corresponds to the difference between the dimer and the sum of monomer energies (i.e., the intramolecular energies have been subtracted out); subscripts QM, elec, and LJ refer to the ab initio, electrostatic, and LJ energies, respectively; and superscript i corresponds to the i -th conformation. The weights w_1^i and w_2^i follow Metropolis-like forms

$$w_k^i = \begin{cases} 1, & \text{if } x_k < 0 \\ \exp(-\beta x_k), & \text{otherwise} \end{cases}$$

where $\beta^{-1} = k_B T_{\text{room}}$ corresponds to thermal energy at $T_{\text{room}} = 300$ K; $k = \{1, 2\}$; and

$$x_1 = \Delta E_{\text{QM}}^i - \Delta E_{\text{elec}}^i \quad (15)$$

$$x_2 = \min(\Delta E_{\text{QM}}^i - \Delta E_{\text{elec}}^i, \Delta E_{\text{LJ}}^i) \quad (16)$$

The weight w_1^i enhances favorable intermolecular LJ energies, as determined from the quantity $\Delta E_{\text{QM}}^i - \Delta E_{\text{elec}}^i$. The second iteration refines the parameters through the weight w_2^i , which corrects for false positives by including conformations with high $\Delta E_{\text{QM}}^i - \Delta E_{\text{elec}}^i$ values but low (i.e., favorable) ΔE_{LJ}^i energies. The Metropolis-like functional form used for both weights hinders high-energy conformations compared to β and focuses instead on the attractive part of the potential. In a similar spirit, a Boltzmann weight was applied to parametrize the LJ parameters of pyridine.⁶³

Pure-Liquid Density. We calculated pure-liquid densities from NPT MD simulations for $N \approx 300$ (depending on the compound), $P = 1$ atm, and T corresponding to the value of the experimental measurement. A 60 ps long warmup run was followed by a 60 ps long production phase, of which we used the last 20 ps to extract the time-averaged box size. This methodology allowed us to obtain relative statistical errors below 3%.

Combined Optimization. LJ parameters were optimized to best reproduce both ab initio calculations (i.e., minimum root-mean-squared error, RMSE, between ab initio and force-field energies) and pure-liquid densities. Out of the parameter sets that fell within 10% of the lowest RMSE observed, the one that provided the most accurate pure-liquid density was retained.

Because we restrain the strength of all monopoles between the PC and MTP parametrizations, the overall electrostatics remain extremely consistent. Thus, we have found it unnecessary to reparametrize the VDW interactions for the MTP force field but rather rely on the set of PC-derived LJ parameters. Finally, we point out that neither the optimized set of PC/MTP nor the LJ coefficients need to be unique—a variety of combinations may reproduce virtually identical ESPs, intermolecular energies, and pure-liquid densities. This characteristic is common among force-field parametrization schemes and need not be worrisome, as long as the resulting model proves effective—as will be shown below.

Fragment-Based Parametrization. The use of the above-mentioned protocol evidently relies on the existence of empirical data. As we are not aware of existing pure-liquid density data for the sulfonamide ligands studied in the present work (Figure 1), we instead performed a fragment-based approach where we selected a list of small, neutral molecules that encompass the entire set of required atom types to parametrize the BZS and SBB ligands (Table 2). We included molecular structures of all fragments with their list of atom types in the Supporting Information (Table S2).

Table 2. Fragments Used in the LJ Parametrization of the BZS and SBB Ligands, as Well as Their Molar Mass, Experimental Density,⁶⁴ and Associated Temperature, and the Atom Type(S) Parametrized

fragment	molar mass [g/mol]	density [g/cm ³]	T_{density} [K]	atom types
benzene	78.1	0.877	293	Car, Har
fluorobenzene	96.1	1.023	293	Fmon
toluene	92.1	0.862	298	Cmet, Hmet
trifluorotoluene	146.1	1.188	293	Cfm, Fmet
ethylbenzene	106.2	0.863	298	Cdm
benzamine	93.1	1.022	293	Nam2, H
N-methylaniline	107.2	0.989	293	Nam1
amidosulfonic acid	97.1	2.15	293	S, O
benzamide	121.1	1.079	403	C

The electrostatic coefficients (whether PC or MTP) of each atom type were optimized by fitting simultaneously all ligands (including various conformations for the long SBB ligands) and fragments. Rather than fitting LJ parameters of all atom types simultaneously, the present LJ parametrization scheme relied on a sequential optimization of compounds, each introducing up to two new atom types at once. Indeed, the time for a single optimization iteration—bound by the NPT simulation time—

refrained us from fitting all parameters simultaneously. While the order in which compounds, and thus atom types, is parametrized inherently biases the results, the method has the advantage of reducing the dimensionality of parameter space and thereby allows for a systematic scan of ϵ_i and R_i^{\min} . Most importantly, we show below that it produces accurate thermodynamics—except for the last fragment parametrized, which is discussed further down. We point out that Cacelli et al. recently proposed a method where all coefficients are fitted simultaneously: a genetic algorithm estimates liquid densities by interpolation/extrapolation of LJ parameters to limit the number of *NPT* simulations.⁶³

RESULTS

Force-Field Validation: Hydration Free Energies.

Optimized LJ coefficients, resulting densities, and RMSEs are shown in Table 3. As a means to validate the PC force field, we

Table 3. List of Optimized LJ Coefficients Derived by Each Fragment^a

fragment	atom type	LJ coefficients		quality of fit	
		ϵ_i	$R_i^{\min}/2$	density	RMSE
benzene	Car	−0.06	2.14	0.887	0.467
	Har	−0.16	0.50		
fluorobenz.	Fmon	−0.13	1.70	1.010	0.881
toluene	Cmet	−0.16	2.00	0.863	0.953
	Hmet	−0.01	1.50		
trifluorotol.	Cfm	−0.05	2.15	1.186	0.862
	Fmet	−0.09	1.70		
ethylbenz.	Cdm	−0.21	1.47	0.861	1.468
benzamine	Nam2	−0.22	2.05	1.027	1.278
	H	−0.01	0.50		
<i>N</i> -methyl.	Nam1	−0.23	1.83	0.975	1.101
amidosulf.	S	−0.11	2.00	2.209	2.199
acid	O	−0.16	1.00		
benzamide	C	−0.34	2.45	1.081	1.066
average RMSE		—	—	—	1.142

^aThe quality of the fit was included in each case for: calculated density (experimental values can be found in Table 2) and RMSE of ab initio energies. The order of compounds parametrized runs from top to bottom. The second column lists the atom type(s) introduced with each compound. Units used throughout: energy [kcal/mol], length [Å], and density [g/cm³].

calculated absolute hydration free energies ΔG_{hyd} of the fragments used in the parametrization and compared them with experimental values (when available). All simulations were run at 298 K (25 °C) and 1 atm, following the experimental conditions. The results, presented in Table 4, show that all calculated ΔG_{hyd} differ by less than 1 kcal/mol of the experimental value, except for benzamide—the last fragment parametrized. We point out that the density of benzamide was measured at 403 K (see Table 2), roughly 105 K higher than all other compounds. Considering that an empirical force-field parametrization is state dependent, it is unlikely that the other atom types previously parametrized will transfer well to that environment. It is thus unclear how well we should expect the force field to perform at such a high temperature. Besides, all attempts to vary the LJ parameters of the single atom type optimized from this compound (i.e., the carbon atom of the carbonyl group, “C”) yielded values of ΔG_{hyd} that were too hydrophobic. This can be rationalized by noting that the

Table 4. Calculated and Experimental (When Available) Hydration Free Energies^a

fragment	$\Delta G_{\text{hyd}}^{\text{calc}}$	$\Delta G_{\text{hyd}}^{\text{exp}}$
benzene	−1.5 ± 0.1	−0.86
fluorobenzene	−0.6 ± 0.1	−0.89
toluene	−1.3 ± 0.1	−0.89
trifluorotoluene	−0.1 ± 0.1	−0.25
ethylbenzene	−0.8 ± 0.2	−0.79
benzamine	−8.4 ± 0.3	—
<i>N</i> -methylaniline	−3.4 ± 0.2	−4.69
amidosulfonic acid	+0.8 ± 0.1	—
benzamide	−1.8 ± 0.4	−11.00

^aExperimental data from ref 65 and references therein. Units used throughout are kcal/mol.

carbonyl group’s polarity is likely to depend heavily on the more exposed oxygen atom. Hence, choosing a different compound measured around room temperature would not have improved things much. Instead, correcting for this outlier would have required a simultaneous parametrization of all atom types. The accuracy of the hydration free energies for the other compounds (for which experimental data were available) and the absence of atom type “C” in our alchemical transformations (below) convinced us that our force field was yet suitable for the present work.

Evaluation of the MTP Scoring Method. Using the PC force field, we performed seven alchemical transformations of the ligands in Figure 1: substitutions between BZS (Figure 1(a)) and any other ligand in the BZS set and substitutions between SBB (Figure 1(f)) and any other ligand in the SBB set. We also attempted to calculate the BZS → SBB transformation but found that our simulation time did not allow for proper convergence of the free energies—a consequence of the large chemical group that needs to be grown in this case. The resulting PC-derived binding free energies $\Delta \Delta G_{\text{bind}}$ are compared to the experimental values $\Delta \Delta G_{\text{bind}}^{\text{exp}}$ in Figure 2. All

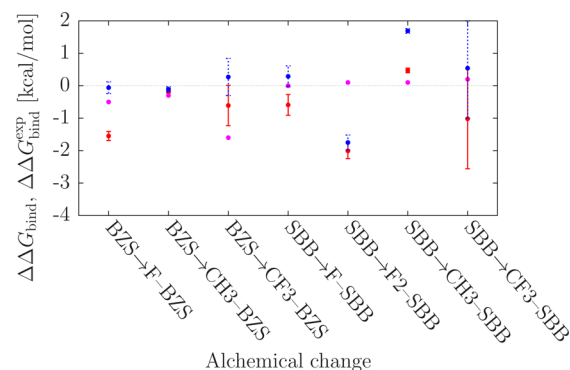


Figure 2. Experimental (magenta points), PC-derived (red, solid lines), and MTP-scored (blue, dashed lines) protein–ligand binding free energies for various ligand substitutions. Experimental error bars, which can be found in Table 1, were not included here for the sake of clarity.

but one substitution fall within 1 kcal/mol of the experimental values, and the error bars are small ($\sigma < 1$ kcal/mol), except for SBB → CF₃-SBB. The outlier, SBB → F₂-SBB, is likely misestimated due to insufficient sampling of the torsional motion of the difluoro-phenyl group, where the fluorine atoms may either point toward the protein pocket or the solvent.

While X-ray crystallography suggests they mostly point toward the solvent,²⁷ the simulation samples both conformations. It is likely that longer simulation times and/or more efficient sampling techniques (e.g., ref 66) would be necessary to obtain a more representative population of conformations.

Overall, our PC-derived protein–ligand binding free energies achieve a level of accuracy of 1.10 kcal/mol on average—in agreement with other computational studies that use similar free-energy calculation techniques.^{67–70} This compares with expected absolute errors of the experimental measurements of 0.5–1 kcal/mol.²⁸

In light of these results, we evidently do not expect significant improvements from force-field refinements. Rather, comparing the PC simulations and the MTP-scored results allows us to check if and when the present method provides reliable results. Remarkably, the MTP-scored results provide error bars of similar magnitude compared to their PC counterpart and a similar average error: 1.19 kcal/mol (2; blue, dashed lines). Indeed, the difference in average error between PC and MTP is negligible considering the systematic errors in the experimental data. The correlation coefficient between the PC and MTP electrostatic energies of each FEP calculation (~6000 data points) was systematically above 0.99 (data not shown), which directly stems from our parametrization protocol: by enforcing the monopoles to remain virtually identical from PC to MTP representations, the higher multipoles are a perturbation to PCs, and thus their influence can be controlled better. We further rationalize these findings by pointing out that hydration free energies—a simple surrogate for protein–ligand binding free energies—are notoriously sensitive to modest changes in VDW radii.⁶² Overall, this demonstrates several points: (i) the large correlation between electrostatic energies obviates the need for a reoptimization of the VDW parameters for the MTP force field; (ii) the moderate variation of $\Delta\Delta G$ between PC and MTP despite the virtually perfect correlation illustrates the exquisite effects of electrostatic parameters on protein–ligand binding free energies; (iii) a careful, consistent parametrization between PC and MTP force fields provides enough transferability to sample with one force field and score energies with the other.

Application: Solvation of C–H and C–F Groups.

Considering the promising results of the MTP scoring method obtained for protein–ligand binding free energies, we set out to study the multipolar electrostatics of C–H and C–F groups when solvated in water. A 5 ns long *NPT* simulation was run for BZS, F-BZS, and SF-BZS—a derivative of BZS with a pentafluorophenyl instead of the phenyl ring—solvated in water. We extracted the energy contribution of each multipole moment $Q_k^{(i)}$ on atom i , $E_{Q_k^{(i)}} = E_{Q_k^{(i)} + \text{env}} - E_{\text{env}}$, where $E_{Q_k^{(i)} + \text{env}}$ is the electrostatic energy of the MTP Q_k of atom i with all the other atoms, subtracted by E_{env} , the electrostatics of the environment alone (i.e., all atoms but i)—this ensures that only the effects of multipole $Q_k^{(i)}$ of atom i remain. From the last 4 ns, we extracted $E_{Q_k^{(i)}}$ for C–H and C–F in BZS and F-BZS/SF-BZS, respectively, every picosecond—well beyond the characteristic autocorrelation time. We recall that our parametrization protocol assigns only monopoles to hydrogens. The Cartesian MTP coefficients are expressed in the atom's local axis system,²² as sketched in Figure 3.

Table 5 shows the energy contribution of each MTP coefficient, where the average and error of the mean were extracted from bootstrap resampling.⁴² Displayed coefficients

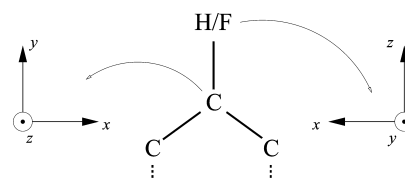


Figure 3. Local axis systems of the 4-carbon (left) and hydrogen/fluorine (right) atoms of the BZS and F-BZS ligands. The carbons and hydrogen/fluorine correspond to axis systems #2 and #6, respectively, as defined in ref 22.

Table 5. Energy Contributions of Individual MTP Moments for the 4-Carbon of BZS (the Attached H Embodies No Nonmonopole Coefficient), 4-Carbon and Attached Fluorine of F-BZS, and 4-Carbon and Attached Fluorine of SF-BZS, a Derivative of BZS with a Pentafluorophenyl Instead of the Phenyl Ring^a

ligand atom	BZS	F-BZS		SF-BZS	
	Car	Car	Fmon	Car	Fmon
MTP	energy	energy	energy	energy	energy
μ_x	—	—	—	—	—
μ_y	+0.193	—	—	+0.057	—
μ_z	—	—	+0.005	—	−0.025
Θ_{xx}	+0.024	—	—	−0.003	—
Θ_{yy}	+0.102	—	—	−0.002	—
Θ_{zz}	−0.126	—	—	+0.005	—
Θ_{xy}	—	—	—	—	—
Θ_{xz}	—	—	—	—	—
Θ_{yz}	—	—	—	—	—

^aOnly results that are statistically significantly different from zero are displayed (i.e., the others are left blank): the error of the mean for each data point, calculated from bootstrap resampling, was less than 0.002 kcal/mol. Dashes correspond to zero contributions due to local planar symmetries. Energies are expressed in kcal/mol.

are statistically significant (i.e., they deviate from zero beyond the error bar). Dashes correspond to zero contributions due to local planar symmetries; e.g., the μ_z coefficient for the aromatic carbons points out of the plane defined by the associated ring—since the transformation $z \rightarrow -z$ would yield the same geometry, the net energy contribution must be zero. Among the atoms we focused on, the 4-carbon of BZS showed several nonzero coefficients: μ_y illustrates the polarization exerted by the C–H bond, and the Θ_{yy} and Θ_{zz} quadrupole moments result from the C–H bond and the typical charge asymmetry normal to benzene rings, respectively. We also observe a weaker, yet statistically significant, Θ_{xx} likely due to the transverse alignment of alternating ESP signs between the neighboring H, C, and H across the x axis. Interestingly, these coefficients vanish—within our calculations' accuracy—for F-BZS, for both the carbon and the fluorine atoms, except for F's μ_z , likely due to the strong electronegativity of fluorine. The small MTP contribution from fluorine indicates that it is well represented by a simple PC, in line with our imposed PC-only hydrogens. As for the carbon of F-BZS, the lack of MTP contributions can simply be explained by the presence of fluorine in a phenyl ring: it is the loss of symmetry in the charge distribution around the carbon that eliminates the contributions of its dipole/quadrupole moments. This effect can directly be visualized from the ab initio ESP (Figure 4): a zero-field node surrounds the fluorine-bound carbon. When substituting all hydrogens of the phenyl ring to fluorines (i.e., SF-BZS), we

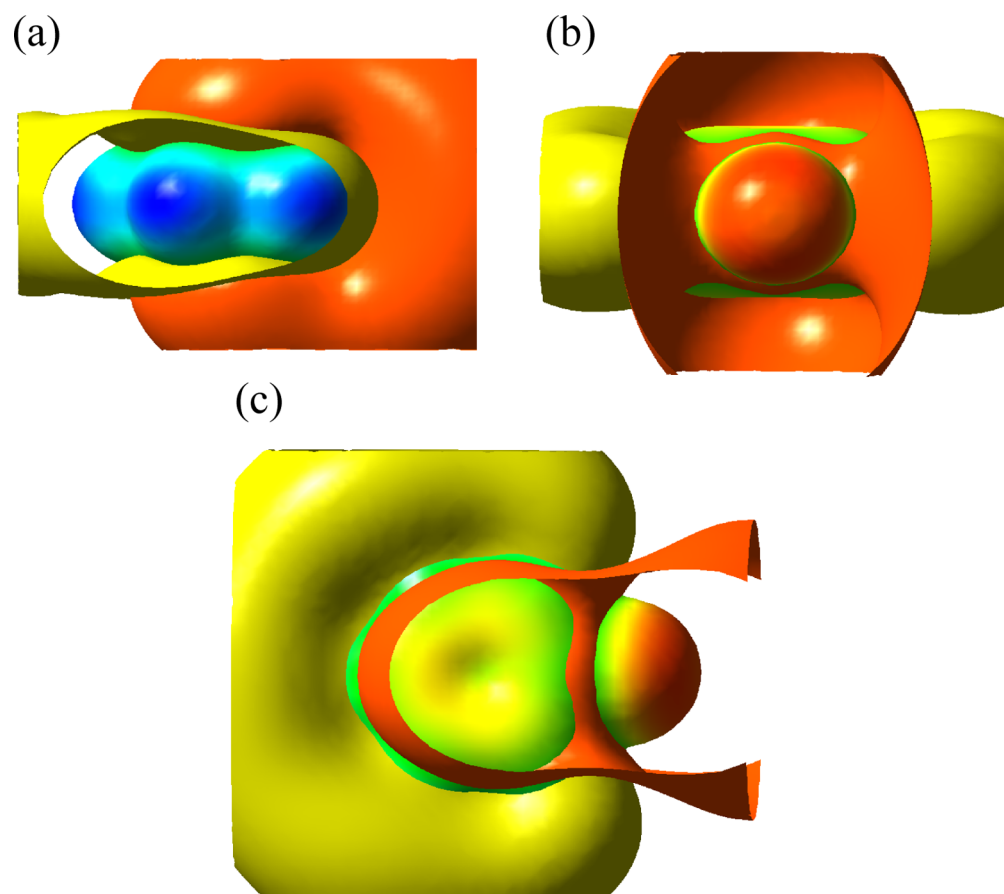


Figure 4. Representation of positive (yellow) and negative (orange) isosurfaces of the ab initio ESP of fluorobenzene along its (a) side view with fluorine to the right, (b) side view with fluorine in front, and (c) top view. Note that a zero-field node surrounds the fluorine-bound carbon. Rendered in GaussView.⁷¹

recover both dipole and quadrupole moments, though most of them are much weaker than for BZS. The signs of the energy contributions can be predicted from a simple analysis of the key interactions. For instance, in the case of BZS, the carbon holds a negative local dipole, i.e., $\mu_y < 0$ (Supporting Information). The dominating electrostatic interactions will occur with the solvent (recall that atomistic force fields turn off electrostatic interactions for bonded neighbors): specifically, the oxygen atoms of the water pointing toward the carbon-bound hydrogen. The partial charge of an oxygen being negative, the resulting energy will have a positive sign, i.e., $E = (-|q|)(-|\mu_y|)\hat{\mu}_y \cdot \hat{r}/4\pi\epsilon_0 r^2 > 0$, where $\hat{\mu}_y \cdot \hat{r}$ provides a positive angular contribution. Overall, we find that significantly contributing multipole moments require some symmetry in the local charge distribution, which is lost in the presence of a single monofluoro-phenyl substituent.

CONCLUSIONS

We demonstrated the applicability of a scoring method to introduce permanent MTP electrostatics in a PC-generated trajectory. The relative accuracy of PC-modeled, computed protein–ligand binding free energies with respect to their experimental counterparts is ≈ 1 kcal/mol. Lowering this number would require improvements in both force fields and experiments. Remarkably, the scoring method retains a virtually identical level of accuracy, provided a consistent parametrization between the two force fields. Achieving this consistency requires additional penalties to the MTP parametrization

scheme, thus degrading the quality of the fit to the ab initio ESP. This prescription is key to ensure the sampling of the same distributions of conformations. Thus, the method will only be applicable when the PC force field is *already* a satisfying approximation, which excludes certain cases such as cation– π systems, where explicit MTP simulations and polarizable force fields are likely to be required.⁷² For more conservative systems, we showed that the method provides insight into the multipolar electrostatics of condensed-phase systems. The computational efficiency of the method allowed us to obtain ample conformational sampling and thereby extract canonically averaged observables. While the absolute values of the individual MTP energies are not very telling (like *any* force-field energy), the relative, statistically significant deviation from 0 of some of them provides a ranking of the important MTP coefficients in describing an atom's interaction with its local environment. We thereby found that the important MTP coefficients of an aromatic carbon in a phenyl ring were very different depending on the atom attached to it: while the symmetry of hydrogens or fluorines around a ring gives rise to both dipole and quadrupole moments, these vanished in the case of the fluorinated carbon in a 4-fluorophenyl (Table 5). A more detailed analysis that links these MTP energetics with the structure of the environment is currently under investigation. Beyond a structural characterization of the electrostatics at play, such an analysis discriminates between important and negligible MTP moments of each atomic site. This information can prove extremely useful in cutting down the number of coefficients

used in future MTP MD simulations, thus significantly reducing its computational costs while maintaining a high level of accuracy.

■ ASSOCIATED CONTENT

■ Supporting Information

Electrostatic parameters (both PC and MTP); structures of the fragments for the parametrization; esterase activity protocol; NMR data for the SBB ligands. This material is available free of charge via the Internet at <http://pubs.acs.org>.

■ AUTHOR INFORMATION

Corresponding Author

*E-mail: bereau@alumni.cmu.edu; m.meuwly@unibas.ch.

Present Address

[§]Institute of General, Inorganic and Theoretical Chemistry, and Center for Molecular Biosciences Innsbruck (CMBI), University of Innsbruck, 6020 Innsbruck, Austria.

Notes

The authors declare no competing financial interest.

■ ACKNOWLEDGMENTS

We thank N. Plattner, D. Andrienko, W. L. Jorgensen, and P. Gedeck for insightful discussions and M. Schmid for providing various scripts and input structures pertaining to the protein–ligand simulations. We also thank C. A. Fierke (U. of Michigan) for providing the hCA II construct.

Work in Basel was supported by the Swiss National Science Foundation (Grant 200020-132406 and the NCCR MUST). C.K. thanks the Novartis Education Office for a Presidential PostDoc Fellowship. F.M. thanks the Novartis Foundation for a fellowship, and E.N. thanks the Marie Curie ITN biotrans FP7-ITN-238531 for financial support.

■ REFERENCES

- (1) Karplus, M.; Petsko, G. A. Molecular Dynamics Simulations in Biology. *Nature* **1990**, *347*, 631–639.
- (2) Wang, W.; Donini, O.; Reyes, C. M.; Kollman, P. A. Biomolecular Simulations: Recent Developments in Force Fields, Simulations of Enzyme Catalysis, Protein–Ligand, Protein–Protein, and Protein–Nucleic Acid Noncovalent Interactions. *Annu. Rev. Biophys. Biomol. Struct.* **2001**, *30*, 211–243.
- (3) Shea, J.-E.; Brooks, C. L., III From Folding Theories to Folding Proteins: a Review and Assessment of Simulation Studies of Protein Folding and Unfolding. *Annu. Rev. Phys. Chem.* **2001**, *52*, 499–535.
- (4) Ponder, J. W.; Case, D. A. In *Protein Simulations*; Daggett, V., Ed.; Advances in Protein Chemistry; Academic Press: New York, 2003; Vol. 66; pp 27–85.
- (5) Klepeis, J. L.; Lindorff-Larsen, K.; Dror, R. O.; Shaw, D. E. Long-Timescale Molecular Dynamics Simulations of Protein Structure and Function. *Curr. Opin. Struct. Biol.* **2009**, *19*, 120–127.
- (6) Best, R. B. Atomistic Molecular Simulations of Protein Folding. *Curr. Opin. Struct. Biol.* **2012**, *22*, 52–61.
- (7) Lindahl, E.; Sansom, M. S. P. Membrane Proteins: Molecular Dynamics Simulations. *Curr. Opin. Struct. Biol.* **2008**, *18*, 425–431.
- (8) Freddolino, P. L.; Arkhipov, A. S.; Larson, S. B.; McPherson, A.; Schulten, K. Molecular Dynamics Simulations of the Complete Satellite Tobacco Mosaic Virus. *Structure* **2006**, *14*, 437–449.
- (9) Zink, M.; Grubmüller, H. Mechanical Properties of the Icosahedral Shell of Southern Bean Mosaic Virus: A Molecular Dynamics Study. *Biophys. J.* **2009**, *96*, 1350–1363.
- (10) Mackerell, A. D. Empirical Force Fields for Biological Macromolecules: Overview and Issues. *J. Comput. Chem.* **2004**, *25*, 1584–1604.
- (11) Caldwell, J. W.; Kollman, P. A. Cation– π Interactions: Nonadditive Effects are Critical in Their Accurate Representation. *J. Am. Chem. Soc.* **1995**, *117*, 4177–4178.
- (12) Politzer, P.; Murray, J. S.; Concha, M. C. σ -Hole Bonding Between Like Atoms; A Fallacy of Atomic Charges. *J. Mol. Model.* **2008**, *14*, 659–665.
- (13) Vinter, J. G. Extended Electron Distributions Applied to the Molecular Mechanics of Some Intermolecular Interactions. *J. Comput.-Aided Mol. Des.* **1994**, *8*, 653–668.
- (14) Dixon, R. W.; Kollman, P. A. Advancing Beyond the Atom-Centered Model in Additive and Nonadditive Molecular Mechanics. *J. Comput. Chem.* **1998**, *18*, 1632–1646.
- (15) Lamoureux, G.; Roux, B. Modeling Induced Polarization With Classical Drude Oscillators: Theory and Molecular Dynamics Simulation Algorithm. *J. Chem. Phys.* **2003**, *119*, 3025.
- (16) Kaminski, G. A.; Stern, H. A.; Berne, B. J.; Friesner, R. A. Development of an Accurate and Robust Polarizable Molecular Mechanics Force Field from ab Initio Quantum Chemistry. *J. Phys. Chem. A* **2004**, *108*, 621–627.
- (17) Ponder, J. W.; Wu, C.; Ren, P.; Pande, V. S.; Chodera, J. D.; Schnieders, M. J.; Haque, I.; Mobley, D. L.; Lambrecht, D. S.; DiStasio, R. A., Jr; et al. Current Status of the AMOEBA Polarizable Force Field. *J. Phys. Chem. B* **2010**, *114*, 2549–2564.
- (18) Stote, R. H.; States, D. J.; Karplus, M. On the Treatment of Electrostatic Interactions in Biomolecular Simulation. *J. Chim. Phys. PCB* **1991**, *88*, 2419–2433.
- (19) Stone, A. J. *The Theory of Intermolecular Forces*; Clarendon Press: Oxford, 1996; Vol. 32.
- (20) Nutt, D. R.; Meuwly, M. Theoretical Investigation of Infrared Spectra and Pocket Dynamics of Photodissociated Carbonmonoxide Myoglobin. *Biophys. J.* **2003**, *85*, 3612–3623.
- (21) Plattner, N.; Meuwly, M. The Role of Higher CO-Multipole Moments in Understanding the Dynamics of Photodissociated Carbonmonoxide in Myoglobin. *Biophys. J.* **2008**, *94*, 2505–2515.
- (22) Kramer, C.; Gedeck, P.; Meuwly, M. Atomic Multipoles: Electrostatic Potential Fit, Local Reference Axis Systems, and Conformational Dependence. *J. Comput. Chem.* **2012**, *33*, 1673–1688.
- (23) Neale, C.; Bennett, W. F. D.; Tieleman, D. P.; Pomès, R. Statistical Convergence of Equilibrium Properties in Simulations of Molecular Solutes Embedded in Lipid Bilayers. *J. Chem. Theory Comput.* **2011**, *7*, 4175–4188.
- (24) Zoete, V.; Meuwly, M.; Karplus, M. Study of the Insulin Dimerization: Binding Free Energy Calculations and per-Residue Free Energy Decomposition. *Proteins* **2005**, *61*, 79–93.
- (25) Krishnamurthy, V. M.; Kaufman, G. K.; Urbach, A. R.; Gitlin, I.; Gudiksen, K. L.; Weibel, D. B.; Whitesides, G. M. Carbonic Anhydrase as a Model for Biophysical and Physical–Organic Studies of Proteins and Protein–Ligand Binding. *Chem. Rev.* **2008**, *108*, 946–1051.
- (26) Schmid, M.; Nogueira, E. S.; Monnard, F. W.; Ward, T. R.; Meuwly, M. Arylsulfonamides as Inhibitors for Carbonic Anhydrase: Prediction & Validation. *Chem. Sci.* **2012**, *3*, 690–700.
- (27) Kim, C. Y.; Chang, J. S.; Doyon, J. B.; Baird, T. T., Jr; Fierke, C. A.; Jain, A.; Christianson, D. W. Contribution of Fluorine to Protein–Ligand Affinity in the Binding of Fluoroaromatic Inhibitors to Carbonic Anhydrase II. *J. Am. Chem. Soc.* **2000**, *122*, 12125–12134.
- (28) Gilson, M. K.; Zhou, H. X. Calculation of Protein–Ligand Binding Affinities. *Annu. Rev. Biophys. Biomol. Struct.* **2007**, *36*, 21–42.
- (29) Zwanzig, R. W. High-Temperature Equation of State by a Perturbation Method. I. Nonpolar Gases. *J. Chem. Phys.* **1954**, *22*, 1420.
- (30) Parenti, M. D.; Rastelli, G. Advances and Applications of Binding Affinity Prediction Methods in Drug Discovery. *Biotechnol. Adv.* **2012**, *30*, 244–250.
- (31) Rühle, V.; Lukyanov, A.; May, F.; Schrader, M.; Vehoff, T.; Kirkpatrick, J.; Baumeier, B.; Andrienko, D. Microscopic Simulations of Charge Transport in Disordered Organic Semiconductors. *J. Chem. Theory Comput.* **2011**, *7*, 3335–3345.

- (32) May, F.; Baumeier, B.; Lennartz, C.; Andrienko, D. Can Lattice Models Predict the Density of States of Amorphous Organic Semiconductors? *Phys. Rev. Lett.* **2012**, *109*, 136401.
- (33) MacKerell, A. D.; Feig, M.; Brooks, C. L. Extending the Treatment of Backbone Energetics in Protein Force Fields: Limitations of Gas-Phase Quantum Mechanics in Reproducing Protein Conformational Distributions in Molecular Dynamics Simulations. *J. Comput. Chem.* **2004**, *25*, 1400–1415.
- (34) Phillips, J. C.; Braun, R.; Wang, W.; Gumbart, J.; Tajkhorshid, E.; Villa, E.; Chipot, C.; Skeel, R. D.; Kale, L.; Schulten, K. Scalable Molecular Dynamics With NAMD. *J. Comput. Chem.* **2005**, *26*, 1781–1802.
- (35) Ryckaert, J. P.; Ciccotti, G.; Berendsen, H. J. C. Numerical Integration of the Cartesian Equations of Motion of a System With Constraints: Molecular Dynamics of n-Alkanes. *J. Comput. Phys.* **1977**, *23*, 327–341.
- (36) Bennett, C. H. Efficient Estimation of Free Energy Differences from Monte Carlo Data. *J. Comput. Phys.* **1976**, *22*, 245–268.
- (37) Shirts, M. R.; Pitera, J. W.; Swope, W. C.; Pande, V. S. Extremely Precise Free Energy Calculations of Amino Acid Side Chain Analogs: Comparison of Common Molecular Mechanics Force Fields for Proteins. *J. Chem. Phys.* **2003**, *119*, 5740.
- (38) Shirts, M. R.; Pande, V. S. Solvation Free Energies of Amino Acid Side Chain Analogs for Common Molecular Mechanics Water Models. *J. Chem. Phys.* **2005**, *122*, 134508.
- (39) Mobley, D. L.; Graves, A. P.; Chodera, J. D.; McReynolds, A. C.; Shochet, B. K.; Dill, K. A. Predicting Absolute Ligand Binding Free Energies to a Simple Model Site. *J. Mol. Biol.* **2007**, *371*, 1118–1134.
- (40) Tembe, B. L.; Cammon, M.; Andrew, J. Ligand-Receptor Interactions. *Comput. Chem.* **1984**, *8*, 281–283.
- (41) Gilson, M. K.; Given, J. A.; Bush, B. L.; McCammon, J. A. The Statistical-Thermodynamic Basis for Computation of Binding Affinities: a Critical Review. *Biophys. J.* **1997**, *72*, 1047–1069.
- (42) Chernick, M. R. *Bootstrap Methods: a Guide for Practitioners and Researchers*; Wiley-Interscience: New York, 2007; Vol. 619.
- (43) Brooks, B. R.; Brooks, C. L.; Mackerell, A. D.; Nilsson, L.; Petrella, R. J.; Roux, B.; Won, Y.; Archontis, G.; Bartels, C.; Boresch, S.; et al. CHARMM: the Biomolecular Simulation Program. *J. Comput. Chem.* **2009**, *30*, 1545–1614.
- (44) Sagui, C.; Pedersen, L. G.; Darden, T. A. Towards an Accurate Representation of Electrostatics in Classical Force Fields: Efficient Implementation of Multipolar Interactions in Biomolecular Simulations. *J. Chem. Phys.* **2004**, *120*, 73–87.
- (45) Monnard, F. W.; Heinisch, T.; Nogueira, E. S.; Schirmer, T.; Ward, T. R. Human Carbonic Anhydrase II as a Host for Piano-Stool Complexes Bearing a Sulfonamide Anchor. *Chem. Commun.* **2011**, *47*, 8238–8240.
- (46) Taylor, P. W.; King, R. W.; Burgen, A. S. V. Kinetics of Complex Formation Between Human Carbonic Anhydrases and Aromatic Sulfonamides. *Biochemistry* **1970**, *9*, 2638–2645.
- (47) King, R. W.; Burgen, A. S. V. Kinetic Aspects of Structure-Activity Relations: the Binding of Sulphonamides by Carbonic Anhydrase. *Proc. R. Soc. London, B: Biol.* **1976**, *193*, 107–125.
- (48) Krishnamurthy, V. M.; Bohall, B. R.; Kim, C. Y.; Moustakas, D. T.; Christianson, D. W.; Whitesides, G. M. Thermodynamic Parameters for the Association of Fluorinated Benzenesulfonamides With Bovine Carbonic Anhydrase II. *Chem.-Asian J.* **2006**, *2*, 94–105.
- (49) Kim, C. Y.; Chandra, P. P.; Jain, A.; Christianson, D. W. Fluoroaromatic-Fluoroaromatic Interactions Between Inhibitors Bound in the Crystal Lattice of Human Carbonic Anhydrase II. *J. Am. Chem. Soc.* **2001**, *123*, 9620–9627.
- (50) Jain, A.; Whitesides, G. M.; Alexander, R. S.; Christianson, D. W. Identification of two Hydrophobic Patches in the Active-Site Cavity of Human Carbonic Anhydrase II by Solution-Phase and Solid-State Studies and their Use in the Development of Tight-Binding Inhibitors. *J. Med. Chem.* **1994**, *37*, 2100–2105.
- (51) Doyon, J. B.; Hansen, E. A. M.; Kim, C. Y.; Chang, J. S.; Christianson, D. W.; Madder, R. D.; Voet, J. G.; Baird, T. A., Jr; Fierke, C. A.; Jain, A. Linear Free Energy Relationships Implicate Three Modes of Binding for Fluoroaromatic Inhibitors to a Mutant of Carbonic Anhydrase II. *Org. Lett.* **2000**, *2*, 1189–1192.
- (52) Grzybowski, B. A.; Ishchenko, A. V.; Kim, C. Y.; Topalov, G.; Chapman, R.; Christianson, D. W.; Whitesides, G. M.; Shakhnovich, E. I. Combinatorial Computational Method Gives new Picomolar Ligands for a Known Enzyme. *Proc. Natl. Acad. Sci. U.S.A.* **2002**, *99*, 1270–1273.
- (53) Iyer, R.; Barrese, A. A.; Parakh, S.; Parker, C. N.; Tripp, B. C. Inhibition Profiling of Human Carbonic Anhydrase II by High-Throughput Screening of Structurally Diverse, Biologically Active Compounds. *J. Biomol. Screening* **2006**, *11*, 782–791.
- (54) Baird, T. T., Jr.; Waheed, A.; Okuyama, T.; Sly, W. S.; Fierke, C. A. Catalysis and Inhibition of Human Carbonic Anhydrase IV. *Biochemistry* **1997**, *36*, 2669–2678.
- (55) Wang, S. C.; Zamble, D. B. Fluorescence Analysis of Sulfonamide Binding to Carbonic Anhydrase. *Biochem. Mol. Biol. Educ.* **2006**, *34*, 364–368.
- (56) Chen, I. J.; Yin, D.; MacKerell, A. D. Combined ab Initio/Empirical Approach for Optimization of Lennard-Jones Parameters for Polar-Neutral Compounds. *J. Comput. Chem.* **2001**, *23*, 199–213.
- (57) Lee, B.; Richards, F. M. The Interpretation of Protein Structures: Estimation of Static Accessibility. *J. Mol. Biol.* **1971**, *55*, 379–400.
- (58) Cornell, W. D.; Cieplak, P.; Bayly, C. I.; Gould, I. R.; Merz, K. M.; Ferguson, D. M.; Spellmeyer, D. C.; Fox, T.; Caldwell, J. W.; Kollman, P. A. A Second Generation Force Field for the Simulation of Proteins, Nucleic Acids, and Organic Molecules. *J. Am. Chem. Soc.* **1995**, *117*, 5179–5197.
- (59) Frisch, M. J.; Trucks, G. W.; Schlegel, H. B.; Scuseria, G. E.; Robb, M. A.; Cheeseman, J. R.; Scalmani, G.; Barone, V.; Mennucci, B.; Petersson, G. A.; et al., *Gaussian 09*, Revision A.1; Gaussian Inc.: Wallingford CT, 2009.
- (60) Jorgensen, W. L.; Maxwell, D. S.; Tirado-Rives, J. Development and Testing of the OPLS all-Atom Force Field on Conformational Energetics and Properties of Organic Liquids. *J. Am. Chem. Soc.* **1996**, *118*, 11225–11236.
- (61) MacKerell, A. D., Jr; Bashford, D.; Bellott, M.; Dunbrack, R. L., Jr.; Evanseck, J. D.; Field, M. J.; Fischer, S.; Gao, J.; Guo, H.; Ha, S.; et al. All-Atom Empirical Potential for Molecular Modeling and Dynamics Studies of Proteins. *J. Phys. Chem. B* **1998**, *102*, 3586–3616.
- (62) Yin, D.; MacKerell, A. D. Combined ab Initio/Empirical Approach for Optimization of Lennard-Jones Parameters. *J. Comput. Chem.* **1998**, *19*, 334–348.
- (63) Cacelli, I.; Cimoli, A.; Livotto, P. R.; Prampolini, G. An Automated Approach for the Parameterization of Accurate Inter-molecular Force-Fields: Pyridine as a Case Study. *J. Comput. Chem.* **2012**, *33*, 1055–1057.
- (64) Lide, D. R. *CRC Handbook of Chemistry and Physics*; CRC press: Boca Raton, FL, 2012.
- (65) Rizzo, R. C.; Aynechi, T.; David, A.; Kuntz, I. D. Estimation of Absolute Free Energies of Hydration Using Continuum Methods: Accuracy of Partial Charge Models and Optimization of Nonpolar Contributions. *J. Chem. Theory Comput.* **2006**, *2*, 128–139.
- (66) Wang, L.; Berne, B. J.; Friesner, R. A. On Achieving High Accuracy and Reliability in the Calculation of Relative Protein-Ligand Binding Affinities. *Proc. Natl. Acad. Sci.* **2012**, *109*, 1937–1942.
- (67) Reddy, M. R.; Erion, M. D. Calculation of Relative Binding Free Energy Differences for Fructose 1,6-Bisphosphatase Inhibitors Using the Thermodynamic Cycle Perturbation Approach. *J. Am. Chem. Soc.* **2001**, *123*, 6246–6252.
- (68) Oostenbrink, C.; van Gunsteren, W. F. Free Energies of Binding of Polychlorinated Biphenyls to the Estrogen Receptor from a Single Simulation. *Proteins* **2003**, *54*, 237–246.
- (69) Michel, J.; Verdonk, M. L.; Jonathan, W. Protein-Ligand Binding Affinity Predictions by Implicit Solvent Simulations: A Tool for Lead Optimization? *J. Med. Chem.* **2006**, *49*, 7427–7439.
- (70) Genheden, S.; Ryde, U. Improving the Efficiency of Protein-Ligand Binding Free-Energy Calculations by System Truncation. *J. Chem. Theory Comput.* **2012**, *8*, 1449–1458.

(71) Dennington, R.; Keith, T.; Millam, J. *GaussView*, Version 5. Semichem Inc.: Shawnee Mission KS, 2009.

(72) Orabi, E. A.; Lamoureux, G. Cation- π and π - π Interactions in Aqueous Solution Studied Using Polarizable Potential Models. *J. Chem. Theory Comput.* **2011**, 8, 182–193.